Dispersal State of Multiwalled Carbon Nanotubes Elicits Profibrogenic Cellular Responses That Correlate with Fibrogenesis Biomarkers and Fibrosis in the Murine Lung

Xiang Wang,[†,‡,#] Tian Xia,[†,‡,#] Susana Addo Ntim,[⊥] Zhaoxia Ji,[‡] Sijie Lin,[†,‡] Huan Meng,[†,‡] Choong-Heui Chung,[§] Saji George,[†,‡] Haiyuan Zhang,[†,‡] Meiying Wang,[†] Ning Li,[†] Yang Yang,[§] Vincent Castranova,[¶] Somenath Mitra,[⊥] James C. Bonner,[∥] and André E. Nel[†,‡,*]

[†]Division of NanoMedicine, Department of Medicine, [‡]California NanoSystems Institute, and [§]Department of Materials Science and Engineering, University of California, Los Angeles, California 90095, United States, [⊥]Department of Chemistry and Environmental Science, New Jersey Institute of Technology, Newark, New Jersey 07102, United States, [∥]Department of Environmental and Molecular Toxicology, North Carolina State University, Raleigh, North Carolina 27695, United States, and [¶]The National Institute for Occupational Safety and Health (NIOSH), 1095 Willowdale Road, Morgantown, West Virginia 26505, United States [#]These authors contributed equally to this work.

ABSTRACT We developed a dispersal method for multiwalled carbon nanotubes (MWCNTs) that allows quantitative assessment of dispersion on profibrogenic responses in tissue culture cells and in mouse lung. We demonstrate that the dispersal of as-prepared (AP), purified (PD), and carboxylated (COOH) MWCNTs by bovine serum albumin (BSA) and dipalmitoylphosphatidylcholine (DPPC) influences TGF-β1, PDGF-AA, and IL-1β production *in vitro* and *in vivo*. These biomarkers were chosen based on their synergy in promoting fibrogenesis and cellular communication in the epithelial–mesenchymal cell trophic unit in the lung. The effect of dispersal was most noticeable in AP- and PD-MWCNTs, which are more hydrophobic and unstable in aqueous buffers than hydrophilic COOH-MWCNTs. Well-dispersed AP- and PD-MWCNTs were readily taken up by BEAS-2B, THP-1 cells, and alveolar macrophages (AM) and induced more prominent TGF-β1 and IL-1β production *in vitro* and TGF-β1, IL-1β, and PDGF-AA production *in vivo* than nondispersed tubes. Moreover, there was good agreement between the profibrogenic responses *in vitro* and *in vivo* as well as the ability of dispersed tubes to generate granulomatous inflammation and fibrosis in airways. Tube dispersal also elicited more robust IL-1β production in THP-1 cells. While COOH-MWCNTs were poorly taken up in BEAS-2B and induced little TGF-β1 production, they were bioprocessed by AM and induced less prominent collagen deposition at sites of nongranulomatous inflammation in the alveolar region. Taken together, these results indicate that the dispersal state of MWCNTs affects profibrogenic cellular responses that correlate with the extent of pulmonary fibrosis and are of potential use to predict pulmonary toxicity.

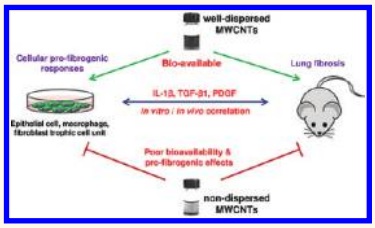

KEYWORDS: multiwalled carbon nanotubes (MWCNTs) · dispersion · TGF-β1 · PDGF-AA · IL-1β · collagen · lung fibrosis

Novel properties of carbon nanotubes (CNTs), including their high mechanical strength, enhanced electrical conductivity, and excellent physicochemical stability, have led to widespread use in electronics, energy storage, sensors, composite materials, and biomedical applications.[1−5] In spite of these enviable characteristics, CNTs also exhibit properties that could render them hazardous under biological conditions.[3,6−10] This includes the ability of multiwalled carbon nanotubes (MWCNTs) to act as bioindestructible fibers in the lung, with the potential to induce pulmonary injury.[6−18] While currently there are no studies showing adverse health effects in workers or consumers, a high level of concern has been raised by animal studies showing that MWCNTs exhibit an equal or greater potential for pulmonary toxicity than crystalline silica and asbestos. For instance, CNTs have been shown to generate early onset and persistent pulmonary fibrosis in short-term and subchronic studies in rodents.[17−20] Moreover, MWCNTs have been observed to migrate from pulmonary alveoli to the pleura where it is theoretically possible that they could induce the development of mesothelioma.[14,16,20]

In addition to their slow rate of clearance from the lung and biopersistance, MWCNTs exhibit a number of properties that could contribute to their ability to induce pulmonary fibrosis.[7,8,21,22] These include the high aspect ratio of the tubes and their relatively high degree of hydrophobicity in the raw state, leading to the formation of tube stacks that are retained as fiber-like substances in pulmonary airways, alveoli, the interstitium, and pleura.[7,8,21,22] From a disease-promoting perspective, longer and more rigid tubes are more prone to generating frustrated phagocytosis in macrophages,

* Address correspondence to anel@mednet.ucla.edu.

Received for review August 26, 2011 and accepted November 2, 2011.

Published online November 02, 2011
10.1021/nn2033055

where the failure to wrap the tubes in phagosomes leads to the release of reactive oxygen species and hydrolytic enzymes that may induce chronic granulomatous inflammation.[8,14,23−27] In addition, activation of the NALP 3 inflammasome and IL-1β production could contribute to the inflammatory response to high aspect ratio materials.[28−30] The extent and localization of inflammation in the lung is dependent on the state of tube dispersal as well as their agglomeration, as illustrated by the finding that better dispersed SWCNTs readily gain access to the alveoli and interstitial space where they generate peri-alveolar fibrosis, while more agglomerated tubes generate granulomatous inflammation and fibrosis in larger airways.[17,18,22,31] Additional CNT characteristics that could contribute to adverse biological outcomes include the tubes' purification stage, content of residual metal catalysts, and surface functionalization (*e.g.*, carboxylation).

Fibrotic reactions in the airways or the lung interstitium constitute a common pathologic outcome following exposure to toxic substances such as inhaled particles, fibers, and metals.[18,22,32−34] There is cumulative understanding of the importance of cooperation among epithelial cells, macrophages, and fibroblasts in the pathogenesis of pulmonary fibrosis.[32−34] Epithelial injury can lead to epithelial−mesenchymal transition (EMT), which represents a graded cellular transformation process in which the epithelial cells acquire reversible mesenchymal features that could culminate in their differentiation to myofibroblasts or fibroblasts.[32,34] The release of chemokines by injured epithelial cells attracts macrophages contributing to EMT through the production of IL-1β, TGF-β1, and proteases.[32] The evolving myofibroblasts and fibroblasts migrate into the space surrounding small airways and alveoli where they deposit extracellular matrix and collagen in amounts proportional to the injurious stimulus as well as the rate and extent at which the mesenchymal elements undergo growth arrest and apoptosis.[32] The production of a family of platelet-derived growth factors (PDGFs) by mesenchymal cells and macrophages plays an important role because these prosurvival factors contribute to the replicative and migratory mesenchymal phenotype at an early stage of fibrosis.[32−34] TGF-β1 is another important growth factor that contributes to collagen synthesis as well as establishing a matrix synthesis phenotype for the mesenchymal cellular elements.[32−34]

We have recently developed a quantitative dispersal technique that allows more directed property−activity analysis of the biological effects of MWCNTs.[35] This included the demonstration that well-dispersed MWCNTs are more robust at inducing TGF-β1 production in epithelial cells as well as sustaining fibroblast proliferation in tissue culture experiments.[35] These findings prompted us to consider whether the state of MWCNT dispersal exerts similar profibrogenic effects in the murine lung. In this communication, we demonstrate significant differences between dispersed and nondispersed, as-prepared, and purified MWCNTs in providing a stimulus for TGF-β1 production in a bronchial epithelial cell line (BEAS-2B) as well as TGF-β1 and PDGF-AA production in lungs of mice receiving MWCNTs *via* oropharyngeal aspiration. Not only did the state of dispersal determine cellular bioavailability and uptake but it also controlled the induction of pulmonary fibrosis in a dose-dependent manner. Better dispersed tubes also induced higher IL-1β production in a human myeloid cell line (THP-1). In contrast, carboxyl-functionalized MWCNTs, although well-dispersed, induced little or no profibrogenic effects in epithelial cells and limited fibrosis in the murine lung. Taken together, these results indicate that the state of dispersal of MWCNTs plays an important role in pulmonary fibrosis by triggering cellular responses originating from the epithelial−mesenchymal trophic cell unit, a modular unit that can be used to explore and predict the fibrogenic effects of this class of nanomaterial *in vivo*.

RESULTS

MWCNT Characterization. Cheap Tubes Inc. supplied the raw or "as-prepared" (AP) MWCNTs, which served as the precursor for preparing purified (PD) and carboxylated (COOH) derivatives as described in our previous study.[35] AP-MWCNTs contained ~5.25 wt % metal impurities from catalysts, which included Ni (4.49 wt %) and Fe (0.76 wt %). These metal catalysts are used during MWCNT synthesis. PD-MWCNTs were obtained by purification that involved dilute acids, chelating agents, and mild conditions so as to not produce oxidized or damaged tubes. This was confirmed by Fourier transform infrared spectroscopy (FTIR), scanning electron microscopy, and energy-dispersive X-ray spectroscopy. After purification, the metal impurities from the tubes decreased from 5.25 to 1.88 wt %. Further acid treatment of the PD-MWCNTs introduced carboxyl groups on 5.27% of the carbon backbone (on a per weight basis); this was confirmed by FTIR. Metal content was not detectable, and sulfate was 0.18 wt %. The basic physicochemical characteristics of this library of MWCNTs are shown in Table 1 as well as Figure S1A and Figure S1B in Supporting Information. Additional details of the MWCNT characteristics appear in a previous publication.[35]

MWCNT Dispersal Determines Bioavailability and Induction of TGF-β1 Production in BEAS-2B Cells. AP-, PD-, and COOH-MWCNTs were stably suspended in BEGM containing bovine serum albumin (BSA) and dipalmitoylphosphatidylcholine (DPPC) as described in our previous study.[35] Figure S1C demonstrates that these dispersants act synergistically to provide good suspension stability, as determined by expressing the absorbance of the tubes remaining in suspension as a % of initial

tube absorbance ($t = 0$) over a 20 h observation period. For biological comparison, we also prepared a set of nondispersed tubes in dispersant-free BEGM. Both the dispersed (D) and nondispersed (ND) tubes were added to BEAS-2B cultures at 10−100 μg/mL and cultured for 24 h, following which the culture supernatants were collected to measure TGF-β1 production. Compared to nondispersed AP- and PD-MWCNTs,

TABLE 1. Physicochemical Characterization of the MWCNTs[a]

MWCNTs	average length (μm)	average diameter (nm)	zeta-potential (mV)	residual impurity (%)	Ni (%)	Fe (%)
AP-MWCNT	10−30	20−30	−25.7	5.25	4.49	0.76
PD-MWCNT	10−30	20−30	−28.1	1.88	1.80	0.08
COOH-MWCNT	10−30	20−30	−48.5	0.18	nd	nd

[a] The average length and diameter of the tubes were measured and analyzed using a TEM microscopy (JEOL 100 CX transmission electron microscope). The zeta-potential was measured using a ZetaSizer Nano-ZS (Malvern Instruments, Worcestershire WR, UK). The elemental compositions of the MWCNTs were determined by energy-dispersive X-ray spectroscopy (EDS, Oxford Instrument, Oxfordshire, UK). The experiment details are described in the Materials and Methods. AP, as prepared; PD, purified; nd, not detected.

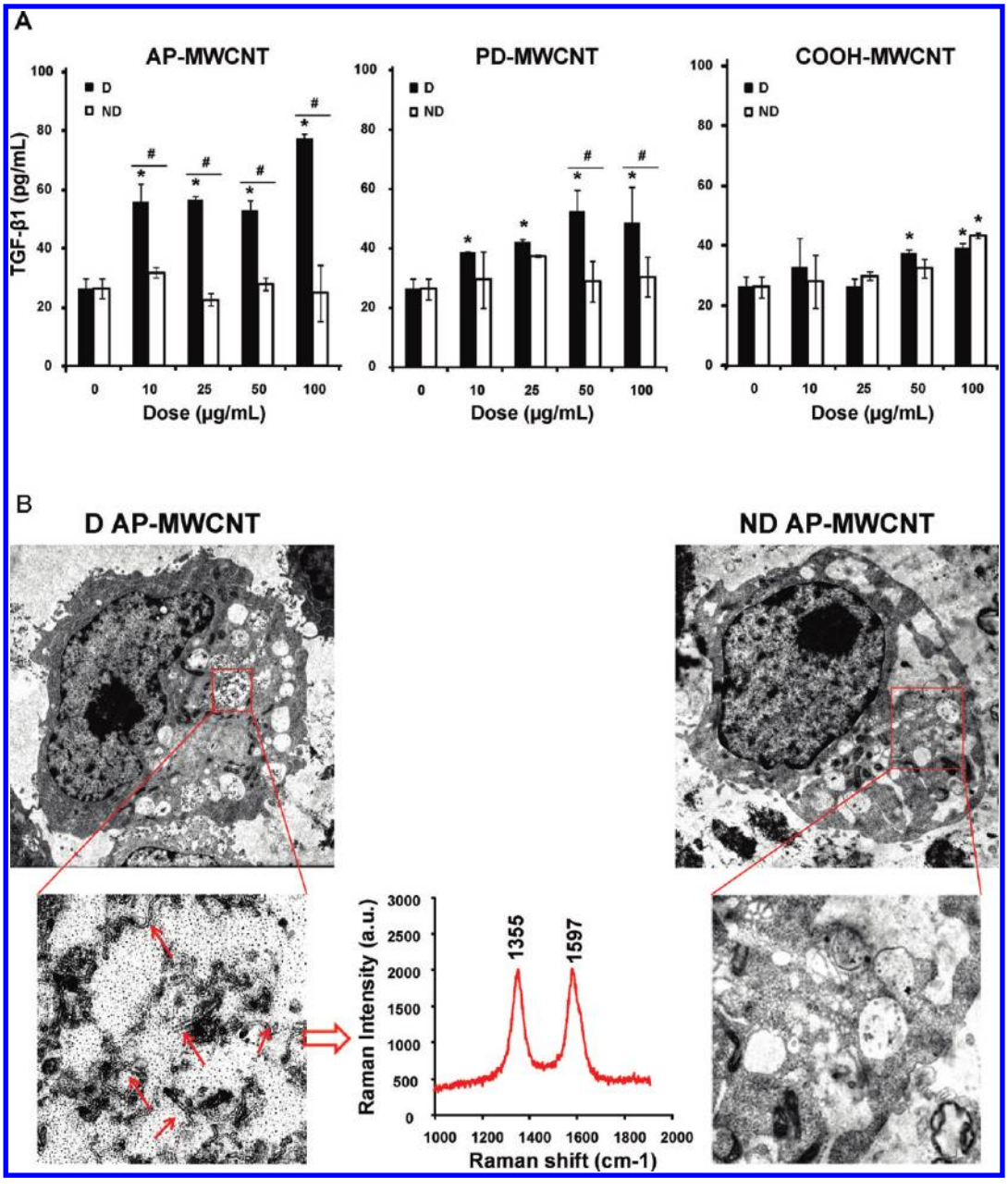

Figure 1. Continued

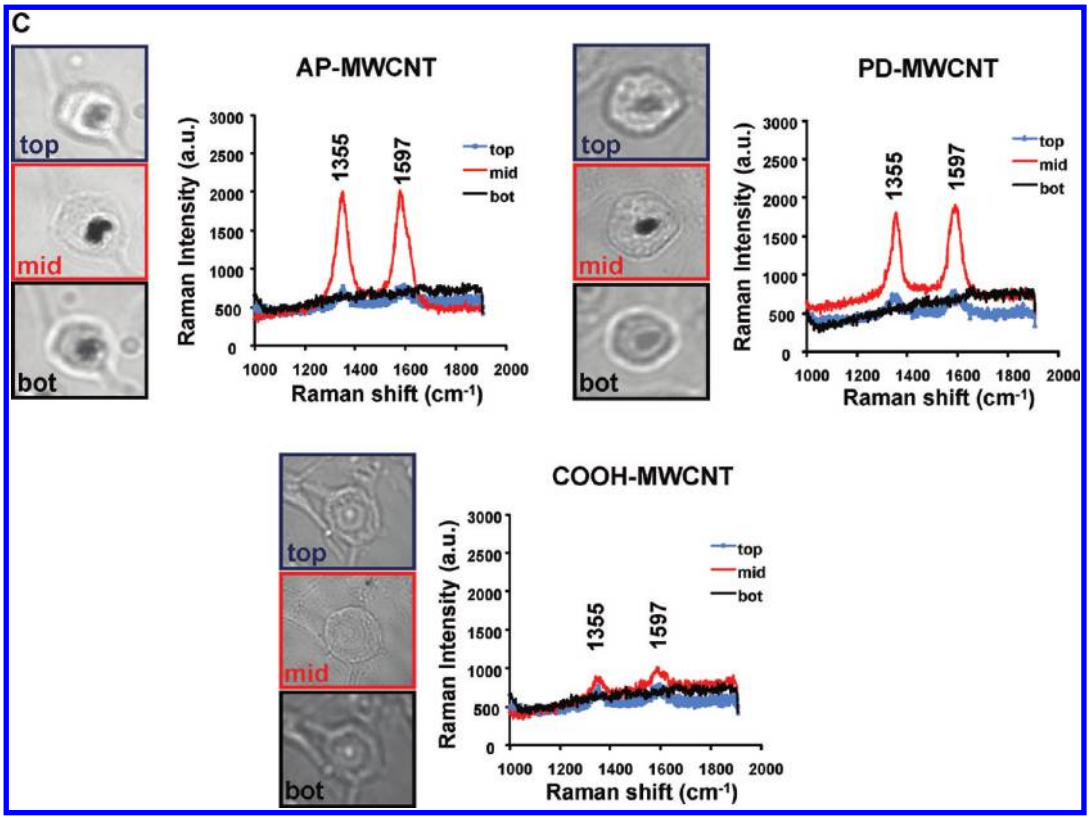

Figure 1. Comparison of the biological effects and uptake of dispersed (D) and nondispersed (ND) MWCNTs in BEAS-2B cells. (A) Cells were treated for 24 h with the indicated concentrations of the AP-, PD-, and COOH-MWCNTs, which were prepared in the presence or absence of BSA (0.6 mg/mL) plus DPPC (0.01 mg/mL) as dispersants. The supernatants were collected to measure the TGF-β1 levels by ELISA as described in Materials and Methods. No significant TGF-β1 production was seen with ND tubes, except at the highest COOH-MWCNT concentration; * denotes a *p* value <0.05, comparing control to CNT-exposed cells; # defines a *p* value <0.05, comparing D to ND tubes. (B) Representative TEM images to show the subcellular uptake of D *vs* ND tubes in cells treated with 50 μg/mL AP-MWCNTs for 24 h. The red arrows point to tubes localized in membrane-lined vesicles. The MWCNT identity was confirmed by the Raman spectroscopy data obtained in a Renishaw inVia Raman microscope system. MWCNTs exhibit characteristic peaks at 1355 and 1597 nm as shown in the middle panel. Identical results were obtained for PD-MWCNTs (Figure S2A). The right side panel shows that ND tubes are not taken up by the cells. (C) Confocal Raman analysis of BEAS-2B cells viewed under a light optic microscope to show quantitative differences in the uptake of well-dispersed AP-, PD-, and COOH-MWCNTs in BEGM over 24 h. Raman microscopy was performed at different cellular planes (top, middle, and bottom) to compare the signal intensities when the beam is focused above, at, or below the cellular localization level of the tubes.

dispersed tubes induced significantly higher TGF-β1 production, particularly in cultures exposed to AP tubes (Figure 1A). In contrast, COOH-MWCNTs were poor inducers of TGF-β1 production and did not show major differences between dispersed and nondispersed tubes (Figure 1A). In order to relate these differences to cellular bio-uptake, we used transmission electron microscopy (TEM) to look for intracellular tubes. Well-dispersed AP- and PD-MWCNTs could be observed in membrane-lined cellular vesicles (Figure 1B and Figure S2A), where the presence of the tubes was authenticated by characteristic MWCNT peaks at 1355 and 1597 nm, using a confocal Raman microscope (Figure 1B and Figure S2A). In contrast, there was little cellular uptake of nondispersed tubes. It was also difficult to visualize uptake of COOH-MWCNTs in either their dispersed or nondispersed state in BEAS-2B cells (Figure S2B). Lower magnification optical microscope images, coupled with confocal Raman analysis, help to further confirm differential bioavailability (Figure 1C). Thus, while well-dispersed AP- and PD-MWCNTs were taken up abundantly, it was difficult to observe a Raman signature for COOH-MWCNTs in BEAS-2B cells (Figure 1C). Together with the data on TGF-β1 production, these results indicate a good correlation between cellular bioavailability and triggering of the profibrogenic response by dispersed *versus* nondispersed tubes.

MWCNT Dispersal Affects IL-1β Production in THP-1 Cells. THP-1 is a human monomyelocytic leukemia cell line that, in response to PMA treatment, differentiates into a myeloid phenotype with phagocytic properties and the ability to initiate IL-1β production in response to long aspect ratio nanomaterials and asbestos fibers.[28] We used THP-1 because this cell line has been utilized as a cellular model for studying inflammasome activation in response to hazardous environmental stimuli.[28] Following exposure to similar doses of dispersed and

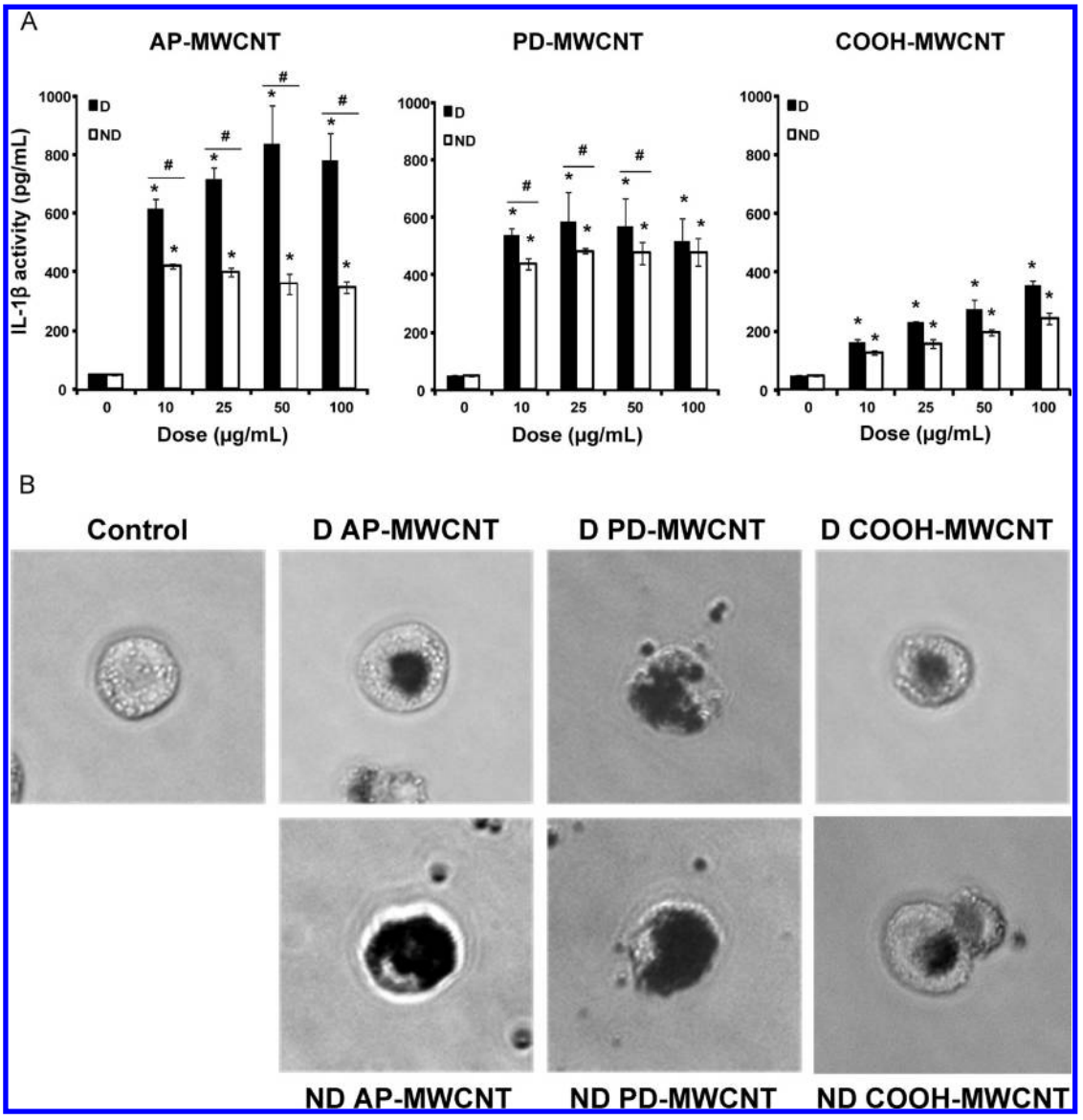

Figure 2. Comparison of the biological effects and uptake of dispersed (D) and nondispersed (ND) MWCNTs in THP-1 cells. (A) Cells were treated for 24 h with the indicated concentrations of the different MWCNTs in their D and ND states as described above. The supernatants were collected to measure the IL-1β production by ELISA as described in Materials and Methods. The * and # symbols denote statistical significance at $p < 0.05$ as described in Figure 1. (B) Representative light optical images looking at cellular uptake of dispersed and nondispersed AP-, PD-, and COOH-MWCNTs. THP-1 cells were treated with D and ND tubes for 24 h and then observed by a phase contrast microscopy (Carl Zeiss, Inc. Peabody, MA, USA).

nondispersed tubes as in Figure 1, THP-1 cells demonstrated a statistically significant augmentation of IL-1β production, with AP-MWCNTs and purified tubes showing more robust responses than COOH-MWCNTs (Figure 2A). In contrast to epithelial cells, all tubes, irrespective of their state of dispersal, were taken up in THP-1 cells, albeit to a lesser degree in the case of COOH-MWCNTs (Figure 2B).

Dose-Dependent Increase in TGF-β1 and PDGF-AA Production in the Lung in Parallel with Increased Fibrosis in Response to Dispersed AP-MWCNTs. The assessment of pulmonary fibrosis is a valid platform for comparing profibrotic effects at the cellular level with similar outcomes in the lung.[18,22,26] First, we asked whether there is any correlation between the bronchoalveolar lavage (BAL) fluid levels of the cytokines and growth factors discussed above and the extent of pulmonary fibrosis. We began with a dose–response study that included the use of dispersed AP-MWCNTs to determine an effective dose for performing the experiments. C57Bl/6 mice received a one-time oropharyngeal aspiration of 0.5, 1, 2, and 4 mg/kg AP-MWCNTs prepared by the addition of dispersants to PBS. The synergistic effect of BSA and DPPC in PBS was demonstrated by assessing the suspension stability index as described above for tissue culture experiments (Figure 3A). Oropharyngeal aspiration of Min-U-Sil was used as positive control. Examination of the BAL fluid showed a dose-dependent

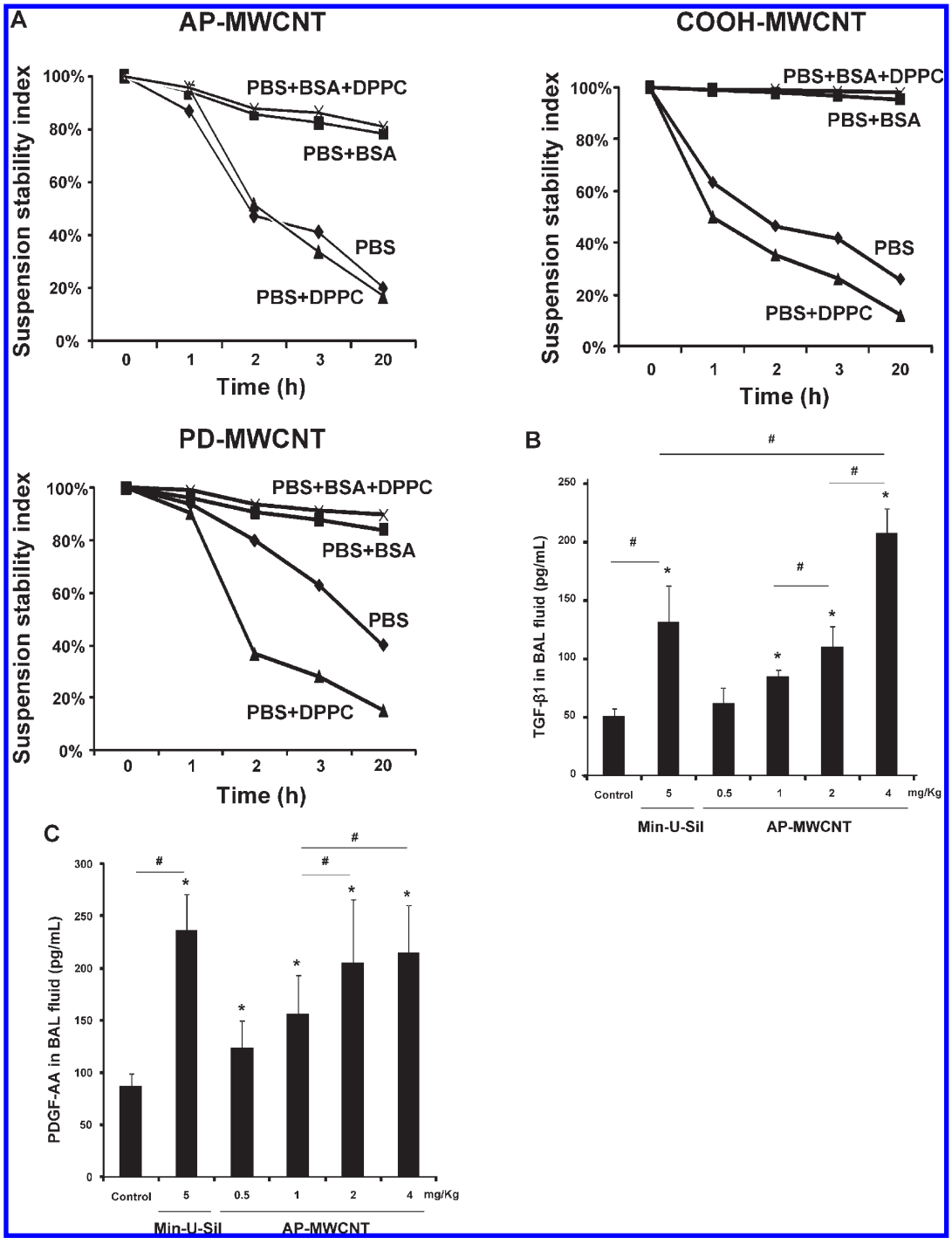

Figure 3. Dose-dependent pulmonary affects of well-dispersed AP-MWCNTs in mice. (A) Assessment of the suspension stability index of the different tube types after their addition at a concentration of 50 μg/mL in PBS, followed by sonication in the absence or presence of 0.6 mg/mL BSA, 0.01 mg/mL DPPC, or a combination of both. The stability index was determined by comparing the initial MWCNT absorbance at $t = 0$ to the absorbance at 1, 2, 3, and 20 h. The absorbance measurements were carried out at $\lambda = 550$ nm in a SpectroMax M5e (Molecular Devices Corp., Sunnyvale, CA) as described in Materials and Methods. (B,C) Anesthetized C57BL/6 mice were exposed one time to well-dispersed AP-MWCNTs at 0.5, 1, 2, and 4 mg/kg by oropharyngeal aspiration. There were 6 animals per group. Animals were euthanized after 21 days, and BAL fluid was collected to determine TGF-β1 (B) and PDGF-AA levels (C). Six mice treated with Min-U-Sil at 5 mg/kg by oropharyngeal exposure served as positive control. TGF-β1 levels were determined by an Emax ImmunoAssay system (Promega, Madison, WI), while PDGF-AA levels were assessed by the Quantikine ELISA kit from R&D Company (R&D Systems, Minneapolis, MN) as described in Materials and Methods. Absorbance was measured at 450 nm using a plate reader (SpectroMax M5e, Molecular Devices Corp., Sunnyvale, CA). The experiment was reproduced a second time; * $p < 0.05$ compared to control, # $p < 0.05$ for pairwise comparisons as shown.

increase in TGF-β1 (Figure 3B) and PDGF-AA (Figure 3C) production in response to well-dispersed AP-MWCNT aspiration at 21 days postexposure. These profibrogenic biomarkers were accompanied by a dose-dependent increase in the collagen content in the lung, as determined by the Sircol collagen assay (Figure 4A). Moreover, we visualized the sites of collagen deposition by Masson's trichrome staining, which demonstrated a dose-dependent increase of collagen content around small airways (Figure 4B). Min-U-Sil also induced TGF-β1 and PDGF-AA production as well as a significant increase in collagen deposition (Figures 3 and 4 and Table 2). IL-1β production in the lung in response to SWCNTs is an early event (*e.g.*, one day) and returns to

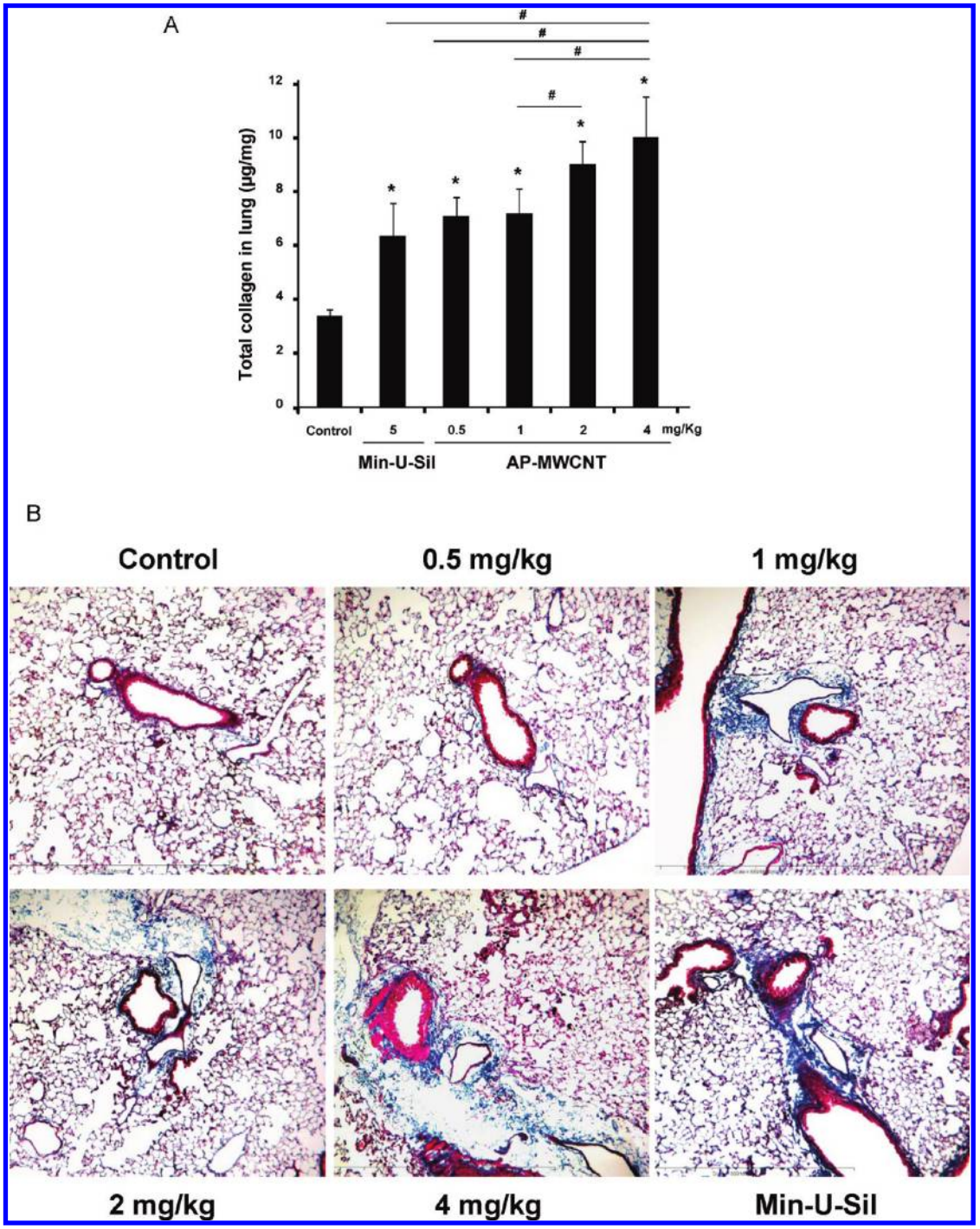

Figure 4. Dose-dependent increase in lung fibrosis, using the organs collected in Figure 3. (A) Total lung collagen content from the same animals as in Figure 3, using a Sircol collagen assay. The experiment was reproduced a second time; * $p < 0.05$ compared with control, # $p < 0.05$ compared among different doses of well-dispersed AP-MWCNTs and Min-U-Sil (positive control). (B) Trichrome staining depicting collagen deposition in the lungs of representative animals treated with dispersed AP-MWCNTs. Lungs were embedded, sectioned, and stained by the Masson's trichrome stain. The red color represents staining of muscle tissue, while collagen is stained blue. Lungs from Min-U-Sil exposed animals served as positive control.

TABLE 2. Morphometric Measures of Airway Fibrosis in Mice Exposed to MWCNTs[a]

treatment	airway intersect score	Area/Perimeter Ratio
control	6.14 + 1.57	3.44 + 0.59
Min-U-Sil	20.25 + 1.70[b]	11.61 + 1.93[b]
AP-MWCNT	D = 16.50 + 2.12[b,c]	D = 12.72 + 1.91[b,c]
	ND = 13.00 + 1.86[b]	ND = 9.69 + 1.47[b]
PD-MWCNT	D = 14.00 + 1.82[b]	D = 9.87 + 0.76[b]
	ND = 13.67 + 3.44[b]	ND = 8.79 + 2.21[b]
COOH-MWCNT	D = 9.75 + 2.06[b]	D = 7.23 + 2.19[b]
	ND = 11.25 + 0.96[b]	ND = 7.31 + 2.47[b]

[a] Airway morphometry was performed using two independent methods: airway intersect scores and area/perimeter ratio. The experiment details are described in the Materials and Methods. AP, as prepared; PD, purified. [b] Significant difference compared to control. [c] Significant difference between dispersed (D) and nondispersed (ND).

basal levels by day 21.[18,32] IL-1β plays a role in the initiation of PDGF-AA production by epithelial cells as well as TGF-β1 production by macrophages at a later stage (days to weeks). Those growth factors act in synergy to induce fibroblast proliferation and collagen deposition in lung.[18,32] Therefore, we also measured IL-1β activity and found that, although the MWCNTs did not result in increased IL-1β levels at 21 days in the BAL fluid compared to the control, we did observe an increase in IL-1β levels at 24 h in an independent experiment in which mice received 2 mg/kg dispersed AP-MWNCTs (Figure S3). This is consistent with previous findings.[18] Min-U-Sil aspiration did result in increased IL-1β production at 21 days (not shown). While Min-U-Sil and MWCNTs induced a small but significant increase in macrophage counts in the BAL fluid, it was interesting to see that at the highest dose MWCNTs were associated with small but significant increases in lymphocyte, neutrophil, and eosinophil counts (Figure S4). The latter finding is interesting from the perspective that the profibrogenic myofibroblast phenotype is occasionally associated with a Th2 lymphocyte phenotype. In this regard, it has been demonstrated that IL-1β production promotes eosinophil recruitment to the lung and can augment PDGF-AA and TGF-β1 production in the context of the epithelial−mesenchymal trophic unit.[32,33] In summary, well-dispersed AP-MWCNTs induced a dose-dependent increase in profibrogenic growth factors in parallel with increased pulmonary collagen deposition. On the basis of this observation, we selected an oropharyngeal dose of 2 mg/kg to perform a comparative analysis of the effects of the three tube types in their dispersed and nondispersed states to see if there is any correlation with the *in vivo* to the *in vitro* profibrogenic events.

Well-Dispersed MWCNTs Elicit Stronger Profibrogenic and Collagen Deposition Effects than Nondispersed Tubes. C57BL/6 mice received a one-time oropharyngeal aspiration of 2 mg/kg AP-, PD-, and COOH-MWCNTs prepared in PBS with and without the use of dispersants. The animals were sacrificed on day 21, and TGF-β1 and

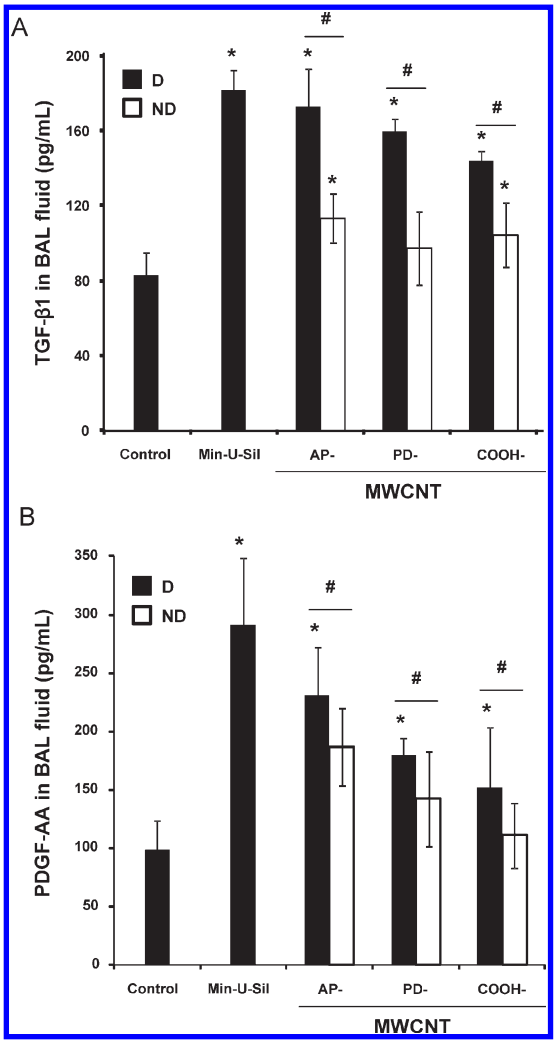

Figure 5. Comparison of the fibrotic effect of AP-, PD-, and COOH-MWCNTs in their dispersed (D) and nondispersed (ND) states. This experiment was performed identical to the experiment in Figure 3, using 6 mice in each group. Oropharyngeal aspiration of a dose of 2 mg/kg AP-, PD-, and COOH-MWCNTs was performed using dispersed (BSA and DPPC) and nondispersed (ND) tube preparations. Twenty-one days after the one-time exposure, the animals were euthanized and BAL fluid collected to determine TGF-β1 levels (A) and PDGF-AA activity (B). Experiment was repeated once, * $p < 0.05$ compared to control, # $p < 0.05$ when comparing D to ND tubes. Mice treated with Min-U-Sil at 5 mg/kg by oropharyngeal exposure served as positive control.

PDGF-AA levels were measured in the BAL fluid as described above. While the well-dispersed tubes induced significantly higher levels of TGF-β1 and PDGF-AA than the nondispersed, there were no significant differences between the tube types except that COOH-MWCNTs yielded nonsignificant lower values (Figure 5A,B). When compared to the quantification of the collagen content in the lung, there was an identical trend in the data spread compared to the growth factor levels, with dispersed tubes resulting in more fibrosis (Figure 6A). While, again, there was less increase in collagen content in response to COOH-MWCNTs, this was not statistically significant (Figure 6A).

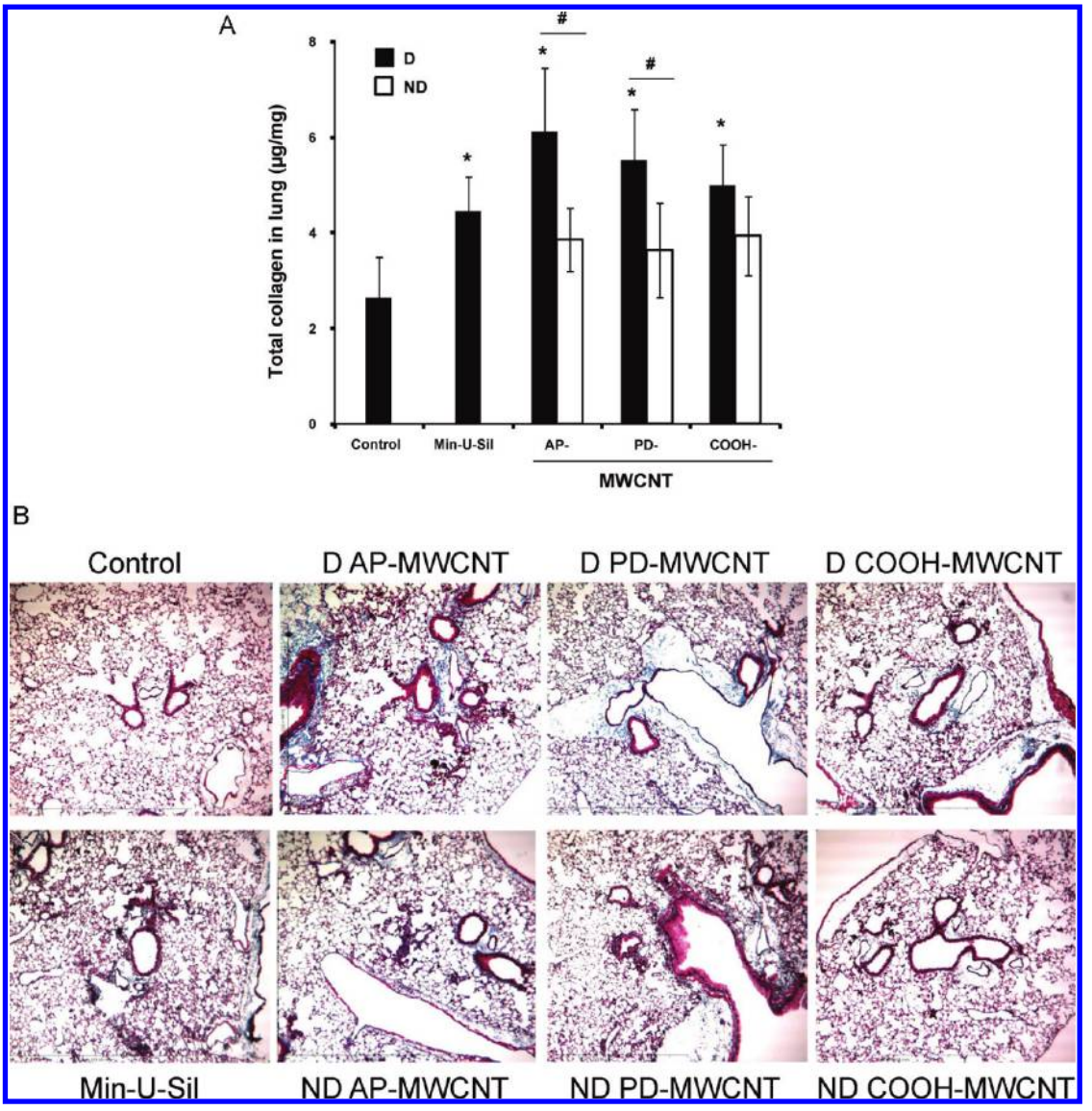

Figure 6. Differential collagen deposition in the lungs of mice for the same experiment shown in Figure 5. (A) Total collagen content of the lung tissue was determined using the Sircol soluble collagen assay kit (Biocolor Ltd., Carrickfergus, UK) as described in the Materials and Methods; * $p < 0.05$ compared with control, # $p < 0.05$ when comparing D to ND tubes. (B) Masson's trichrome staining to assess the tissue distribution of collagen in the lungs as described in Figure 4. These lung images obtained at 100× magnification are representative of the animals in each group. More prominent collagen deposition is seen in animals exposed to D *vs* ND tubes.

However, in trichrome-stained lung sections, it was visually clear that dispersed AP- and PD-MWCNTs induced more prominent peri-bronchiolar and interstitial collagen deposition than COOH-MWCNTs (Figure 6B). The observed increased in trichrome-positive collagen staining around small airways was also quantified using two independent methods that assess airway collagen thickness.[36,37] Both methods showed a significant increase in airway fibrosis caused by MWCNT exposure and confirmed that dispersed AP-MWCNT caused significantly more airway collagen deposition compared to nondispersed tubes (Table 2). Although there are no significant differences between dispersed and nondispersed PD- and COOH-MWCNTs using morphometry analysis, this technique does not take into account the interstitial collagen deposition that is more extensive in the alveolar area for COOH-MWCNTs. In fact, high-resolution hematoxylin and eosin-stained images from the same lung sections demonstrated that, while dispersed AP-MWNCTs are more frequently localized in areas of granulomatous inflammation (Figure 7), COOH-MWCNTs are predominantly localized in granuloma-free sites in the alveoli, with the majority of tubes engulfed by macrophages (Figure 7). Confocal Raman microscopy showed characteristic MWCNT peaks, thus confirming the presence of tubes in these lung areas (see the spectrum B in the Raman insets in Figure 7). PD-MWCNTs also localized at predominant sites of granulomatous inflammation (Figure S5). High-magnification trichrome-stained lung images confirmed that collagen deposition for AP- and

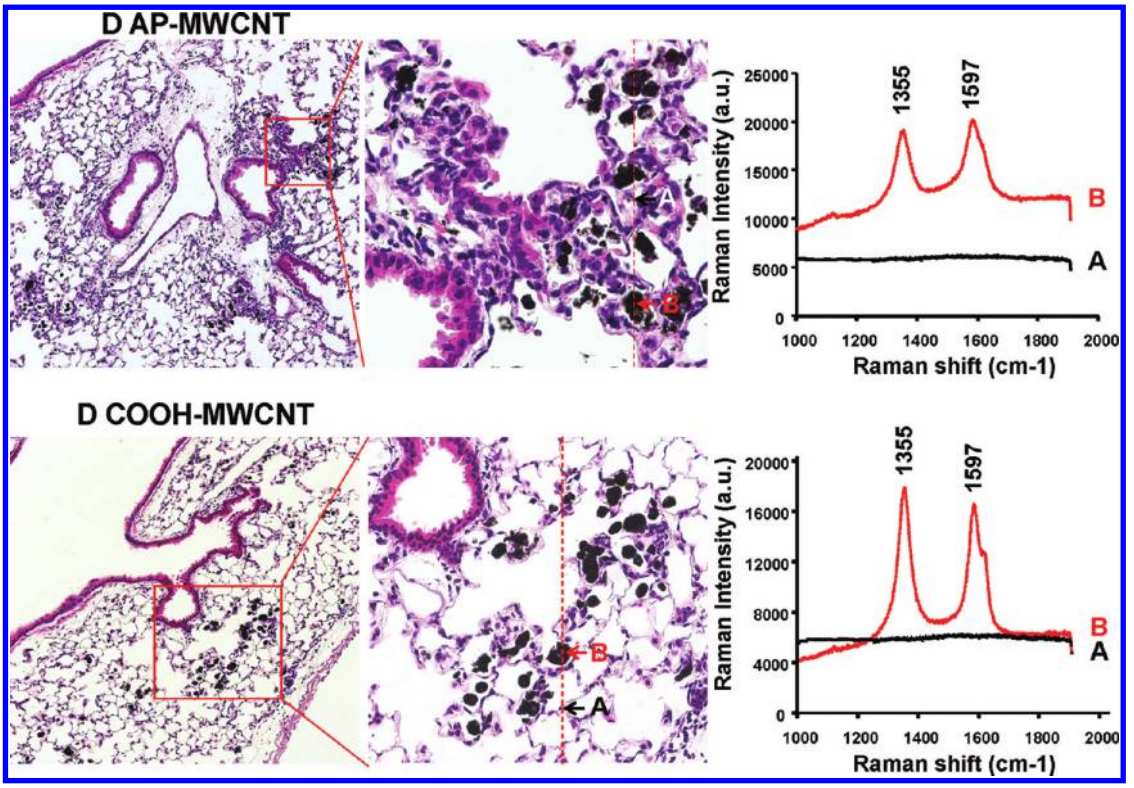

Figure 7. Confocal Raman analysis of the dispersed MWCNTs in the lung. The lung sections were obtained from the same experiment as in Figure 5 and stained with hematoxylin and eosin. Lower (100×) and higher (400×) magnifications are shown of representative regions in the lungs of AP- and COOH-MWCNT exposed animals. PD-MWCNTs had similar effects than AP-MWCNTs. The same lung sections were analyzed in a Renishaw inVia Raman microscope system. Two representative spots in each high-magnification image were chosen for Raman scanning, namely, a spot in an area of granulomatous inflammation for AP-MWCNTs and an alveolar impact site for COOH-MWCNTs. Arrow A is a representative cell not engulfing the MWCNTs, while arrow B denotes a representative cell that loaded with MWCNT. The right panel shows the corresponding Raman spectra identifying the specific peaks at 1355 and 1597 nm.

PD-MWCNTs took place in the setting of granulomatous inflammation, while COOH-MWCNTs stimulate collagen production mostly in the alveolar region (Figure S6). Although not taken up by BEAS-2B cells (Figure S2B), COOH-MWCNTs are engulfed by alveolar macrophages and appear to be quite capable of promoting less but detectable amounts of collagen deposition in this locality. The engulfment of all MWCNT types by pulmonary macrophages was further confirmed by the examination of the BAL fluid (Figure S7). Min-U-Sil induced peptide growth factor production and collagen deposition in accordance with its known profibrogenic effects (Figures 5 and 6).

In an independent study undertaken in the laboratory of Bonner, the investigators performed a comparative analysis of the effects of dispersed AP-, PD-, and COOH-MWNCNTs at days 1 and 21 on biomarker generation in relation to pulmonary fibrosis. This study was performed with oropharyngeal aspiration of 2 mg/kg of tubes as described above, and the results are depicted in the Supporting Information data section (Figures S3, S8A, and S8B). In brief, all tube types induced an increase in the BAL fluid levels of IL-1β on day 1 but not on day 21 (Figure S3). Conversely, all tubes induced a significant increase of TGF-β1 levels on day 21 but not on day 1 (Figure S8A), while for PDGF-AA, the results were mixed with AP-MWCNTs inducing an increase on both days while PD-MWCNTs only induced a response at day 21 and COOH-MWCNTs no significant effect at either time point (Figure S8B).

Taken together, the above data confirm the excellent correlation between the dispersal status of MWCNTs and their relationship to biochemical markers of fibrogenesis in the BAL fluid and collagen deposition in the lung. Moreover, the differences in IL-1β and peptide growth factor production of at different time periods are in accordance with the dynamic evolution of the cellular crosstalk events among the different cell types participating in the epithelial–mesenchymal cell trophic unit.

DISCUSSION

In this study, we demonstrate that the state of dispersal of a small library of MWCNTs from the same precursor induced prominent profibrogenic effects that reflect the cooperation of epithelial and mesenchymal cell elements in the generation of pulmonary fibrosis. The detectable biomarkers, including TGF-β1, PDGF-AA, and IL-1β, act synergistically in the

interim period during which epithelial–myofibroblast transition contributes to collagen deposition in the lung. The effects of tube dispersal were most noticeable for as-prepared (AP) and purified (PD) MWCNTs, which are more hydrophobic and less stable in biological fluids than more hydrophilic COOH-MWCNTs. While carboxyl-functionalized tubes were poorly taken up in BEAS-2B cells and induced little or no TGF-β1 production *in vitro*, they were taken up by lung macrophages and could induce IL-1β and TGF-β1 production *in vivo* along with a discernible increase in collagen deposition around the alveoli. Instead, well-dispersed AP- and PD-MWCNTs were taken up by BEAS-2B cells, THP-1 cells, and alveolar macrophages and induced prominent TGF-β1 and PDGF-AA production in the lung in parallel with prominent granulomatous inflammation and fibrosis around small airways. Nondispersed versions of the same materials induced significantly less TGF-β1 and PDGF-AA production *in vivo* along with reduced pulmonary fibrosis; this was in agreement with reduced IL-1β and TGF-β1 production *in vitro*. Taken together, these results indicate that the state of MWCNT dispersal influences profibrogenic epithelial and macrophage responses that correlate with the extent and localization of pulmonary fibrosis. These findings are of considerable importance in developing a model that relates the biophysical–chemical properties of CNTs at the *in vitro* nano/bio interface to *in vivo* biological outcomes. This could lead to a facilitated method for the assessment of CNT safety.

While the state of dispersal of SWCNTs has been shown to impact the extent and localization of pulmonary fibrosis,[18,22,31] this is the first demonstration that MWCNT dispersal determines the extent to which they initiate fibrogenic effects in epithelial cells and macrophages and where these cellular effects are directly predictive of the extent of pulmonary fibrosis in intact animals. This progress was made possible by the development of a quantitative dispersal technique that uses BSA and DPPC to obtain stable MWCNT suspensions to probe biological events at the nano/bio interface.[31,35,38] In a previous study, we have shown that the dispersal state of MWCNTs exerts prominent effects on fibroblast proliferation and hypothesized that similar biological effects could help to explain disease pathogenesis in the intact lung.[35] While the idea of an improved dispersal state allowing tube access to more distal lung regions is relatively straightforward, it is less clear how the state of dispersal affects bioavailability and triggering of injurious biological effects that result in disease outcome. In the latter instance, the scientific explanation is less obvious as illustrated by the response differences and variation in tube bioprocessing by epithelial cells and macrophages. While it is possible with high-resolution techniques, such as electron microscopy, to show the presence of occasional MWCNTs embedded in the membrane of bronchial or alveolar epithelial cells *in vivo*,[26] we could not directly demonstrate in our histochemistry and Raman studies that there is a prominent epithelial uptake in the intact lung. We did observe clear differences, however, between the ability of dispersed and nondispersed tubes to induce TGF-β1 production in BEAS-2B cells as well as in the experiments looking at IL-1β production in THP-1 cells (Figures 1A and 2A). The same was true when doing a related comparison of the effects of dispersed *versus* nondispersed tubes on growth production in the lung (Figure 5). Thus, while tube dispersal affects cellular uptake, the precise explanation for the triggering of profibrogenic responses remains obscure. One possibility is that coating of the tube surfaces with BSA and DPPC establishes surface ligands that promote cellular contact and/or uptake.[11] It is interesting that SWCNT dispersal by Pluronic F108 leads to good tube dispersal and widespread dissemination throughout the lung.[39] However, under these experimental conditions, the well-dispersed tubes can be cleared from the lung without fibrosis, while nondispersed tubes are retained and induce granulomatous inflammation.[39] It is possible, therefore, that coating of CNTs by the block copolymer introduces steric hindrance that interferes in cellular uptake, compared to coating with BSA and DPPC that promotes cellular bioprocessing and uptake.[39] However, these results do not fully explain why carboxylation of the MWCNT surface leads to less cellular and pulmonary effects when coated with BSA and DPPC. While it is known that the aspect ratio, length, and rigidity of MWCNTs play a role in frustrated phagocytosis and the generation of chronic granulomatous inflammation,[8,23,40,41] we did not observe the classical features of frustrated phagocytosis in our study. Instead, we observed that IL-1β production in THP-1 cells is affected by the state of tube dispersal. Since it is known that the release of this cytokine from myeloid cells and macrophages is dependent on the cleavage of pre-IL-1β by the NALP 3 inflammasome,[28] it is possible that MWCNT dispersal may affect the assembly of inflammasome components through a pathway that includes phagosome or lysosome injury. This aspect is currently under investigation but will require expansion of the CNT properties in our library, including the addition of different tube lengths to perform more detailed property–activity analysis. Being able to pinpoint the exact mechanism of CNT injury in relation to specific tube properties is of key importance for the development of CNT-based therapeutics and imaging agents.

This communication is of considerable importance to the development of *in vitro* assessment tools for hazard assessment and planning of the *in vivo* toxicological testing of CNTs. Several toxicology studies in rodents have been carried out by using intratracheal instillation, oropharyngeal aspiration, or inhalation of

SWCNTs and MWCNTs.[6,15,17,18,21,22] Collectively, these studies have shown a consistent toxicological outcome in terms of pulmonary inflammation and fibrosis, irrespective of the exposure route. The same studies have also demonstrated that some CNT formulations induce more rapid pulmonary fibrosis or at a lower mass burden than either ultrafine carbon black or quartz.[6,16,18] Thus, it is important to develop toxicological assays that can differentiate between the variety of CNT formulations being employed in electronics, solar cells, super capacitors, reinforced plastics, composite materials, aircraft components, biosensors, and pharmaceutical/biomedical devices. As these products make their way to the marketplace, it is important to have test strategies for *in vitro* and *in vivo* hazard assessment. Since the cost of animal studies is high and raises ethical barriers, alternative test strategies are an important consideration. The use of a set of biochemical markers that closely reflect the synergy between macrophages and cellular elements in the epithelial–mesenchymal trophic unit could constitute a screening platform for the rapid and high content data generation that facilitates a predictive toxicological approach.[42] Predictive screening platforms could facilitate decision-making about CNT pulmonary hazard and could evolve, over time, into an independent test platform depending on the stringency of the safety analysis that is accepted by the regulatory community.[42–44] Another advantage of a predictive toxicological platform is the potential to develop high-throughput screening approaches that can assist in the establishment of quantitative structure–activity relationships and the safe design of CNTs for biomedical use. In this regard, we have already demonstrated that high-throughput screening is useful for the assessment of metal and metal oxide nanoparticle toxicity, including the development of safer ZnO nanoparticles.[42,44] Thus, our future efforts will concentrate on developing a high-throughput system that utilizes cellular elements in the epithelial–mesenchymal trophic unit to develop a multiparametric assay to look at synergistic cytokine/growth factor responses. We will compare the use of such an assay to similar biomarkers in BAL fluid and the assessment of pulmonary fibrosis to develop a robust, predictive assessment tool. However, until such testing is available, all possible steps should be taken to minimize CNT exposures in workers.

In order to evaluate the relevance of the *in vivo* findings in mice to human MWCNT exposures, it is interesting to perform an extrapolation of the doses used in mice to possible occupational exposures in humans. The MWCNT doses of 0.5, 1, 2, and 4 mg/kg used in our experiment equal 12.5, 25, 50, and 100 μg per mouse as addressed in the Materials and Methods section. Han *et al.* reported peak MWCNT-containing airborne dust levels being as high as 400 $\mu g/m^3$ in a MWCNT production laboratory.[44] On the basis of this finding, Porter *et al.* calculated that a worker exposed to MWCNT for 8 h/day over a month at 400 $\mu g/m^3$ would carry a lung burden equivalent to a mouse receiving 10 μg MWCNT by aspiration.[20] Therefore, in a worse case scenario, lung burdens of 12.5–100 μg per mouse lung (alveolar surface area, 0.05 m^2 per animal) is equal to a human lung (102 m^2 alveolar surface area) burden that can be acquired following 1.25 to 10 months of exposure.[45] Assuming a 10-fold lower exposure level (40 $\mu g/m^3$), mouse lung burdens will be equivalent to 1–10 years of exposure in human in a contaminated work place. Thus, these estimates suggest that the MWCNT doses tested in mice in this study approach realistic occupational exposures in humans.

The dose–response relationships leading to the generation of pulmonary fibrosis in rodents has served as the scientific basis for the National Institute of Occupational Safety and Health (NIOSH) draft recommending an exposure limit (REL) of 7 $\mu g/m^3$ in CNT exposure environments.[47] This draft's recommended exposure limit was developed based on available acute and subchronic animal exposure studies linking early stage fibrosis and inflammatory responses in the lung to CNT dose. Benchmark dose (BMD) estimates were calculated by using species differences in alveolar lung surface area, which has been estimated to be 0.05 and 102 m^2 in the mouse and human lung, respectively.[46] Therefore, exposure to 50 μg of CNTs would normalize to a surface area dose of 0.1 $\mu g/cm^2$ in the murine lung; this is equivalent to a human lung burden of 102 mg. The REL of 7 $\mu g/m^3$ was calculated based on the expected retained alveolar dose in workers being exposed 8 h per day, 40 h per week, 50 weeks per year, and over a 45 year working lifetime. Please notice that although the draft REL is set at the lowest airborne CNT concentration that can be accurately measured by NIOSH methodology, an excess risk of adverse lung effects is still possible below this level and efforts should be made to reduce airborne concentrations of CNTs as low as possible.

Extrapolation of *in vitro* to *in vivo* dosimetry remains a daunting challenge in ENM toxicology but can be initially approached by normalizing the MWCNT surface area dose in the tissue culture dish to the normalized surface area dose in the rodent airways. Assuming that the entire MWCNT dose of 10–100 μg/mL in the tissue culture dish is bioavailable, this translates to an *in vitro* surface area dose of 3.1–31.2 $\mu g/cm^2$. If we assume that the same exposure dose is evenly deposited in the lung, this would constitute an alveolar surface area exposure of 0.025–0.2 $\mu g/cm^2$, providing a departure point for reconciling *in vitro* and *in vivo* dose calculations. To allow such comparisons, this will require the calculation of bioavailable cellular and tissue dose, necessitating some type of tube labeling to perform those estimates. Moreover, we have to consider that the *in vitro* exposure takes place over a 24 h time period compared to *in vivo*

exposure being performed over 21 days. Thus, we also need to assess the fraction of tubes that are retained in the lung *versus* those that are cleared. Finally, it is appropriate to consider whether a mass-based dosimetry system is appropriate or should be supplemented by dosimetry calculation that takes into consideration the toxicological mechanism by developing quantitative property–activity relationships.

MATERIALS AND METHODS

Carbon Nanotubes and Chemicals. A powdered MWCNT stock was purchased from Cheap Tubes Inc. (Brattleboro, VT, USA). The starting raw material is also being referred to as-prepared (AP) MWCNTs. Bronchial epithelial growth medium (BEGM) was obtained from Lonza (Mapleton, IL, USA), which is supplemented with a number of growth factors, including bovine pituitary extract (BPE), insulin, hydrocortisone, hEGF, epinephrine, triiodothyronine, transferrin, gentamicin/amphotericin-B, and retinoic acid. Roswell Park Memorial Institute medium 1640 (RPMI 1640) was purchased from Invitrogen (Carlsbad, CA, USA). Low-endotoxin bovine serum albumin (BSA) and fetal bovine serum (FBS) were from Gemini Bio-Products (West Sacramento, CA, USA). Dipalmitoylphosphatidylcholine (DPPC) was purchased from Sigma-Aldrich (St. Louis, MO, USA). Min-U-Sil was obtained from U.S. Silica (Frederick, MD, USA). All MWCNT stock solutions were prepared using pure deionized water (DI H_2O) with resistivity >18 MΩ-cm.

Physicochemical Characterization of MWCNTs. The purification and functionalization of the MWCNTs were accomplished as previously described.[35,48−50] A number of techniques were used to characterize MWCNTs, including energy-dispersive X-ray spectroscopy (EDS, Oxford Instrument, Oxfordshire, UK) to identify the elemental composition of the tubes. Zeta-potential measurements of the tube suspensions were performed using a ZetaSizer Nano-ZS instrument (Malvern Instruments, Worcestershire WR, UK). The average length and diameter of the tubes were measured under a TEM microscopy (JEOL 100 CX transmission electron microscope).

Preparation of MWCNT Suspensions in Media. AP-, PD-, and COOH-MWCNTs were provided as dry powders. The samples were weighed in the fume hood on an analytical balance and suspended in distilled, deionized H_2O at a concentration of 5 mg/mL in 4 mL glass vials. These suspensions were sonicated for 15 min in a water sonicator bath (Branson, Danbury, CT, USA, model 2510, 100 W output power; 42 kHz frequency) and used as the stock solution for further dispersion in cell culture media or PBS. A sonicator bath rather than a sonication probe was used to deliver a cavitation force suitable for deagglomeration but not too high to disrupt protein attachment or induce tube damage.[9,51,52] An appropriate amount of each stock solution was added to the desired final concentration in cell culture media or PBS. BSA and DPPC were added to the culture media or PBS at 0.6 and 0.01 mg/mL, respectively, before the addition of the MWCNTs. The diluted tube suspensions were vortexed for 15 s (fixed-speed vortex, 02-215-360, Fisher Scientific, Pittsburgh, PA, USA), sonicated for 15 min, and then vortexed for another 15 s to obtain well-dispersed tube suspensions at the desired final concentrations. The nondispersed tubes were similarly processed in the absence of dispersants.

Cellular Culture and Co-incubation with MWCNTs. BEAS-2B and THP-1 cells were obtained from ATCC (Manassas, VA). BEAS-2B cells were cultured in BEGM at 5% CO_2 and 37 °C. Before MWCNT exposure, aliquots of 1×10^4 cells were cultured in 0.2 mL of BEGM in 96-well plates (Costar, Corning, NY) at 37 °C overnight. All of the MWCNT solutions were freshly prepared at final concentrations of 10, 25, 50, and 100 μg/mL in BEGM. While nondispersed MWCNTs were sonicated in BEGM devoid of dispersants, well-dispersed MWCNTs were prepared by sonication in BEGM containing 0.6 mg/mL BSA plus 0.01 mg/mL DPPC before addition to the tissue culture plates. THP-1 cells were cultured in RPMI 1640 medium supplemented with 10% fetal bovine serum. Before MWCNT exposure, THP-1 cells were pretreated with 1 μg/mL phorbol 12-myristate acetate (PMA) for 18 h and primed with 10 ng/mL lipopolysaccharide (LPS) to initiate transcription of the IL-1β precursor. Aliquots of 1.5×10^4 primed cells were seeded in 0.2 mL of complete medium in 96-well plates (Costar, Corning, NY, USA). For preparing the tube suspension, MWCNTs were added to complete RPMI 1640 at final concentrations of 10, 25, 50, and 100 μg/mL. The suspensions were treated with dispersants and sonicated in the absence of dispersants as described above. Following exposure to the tubes for 24 h at 37 °C, the supernatants were collected and used to measure TGF-β1 and IL-1β production.

Cellular Transmission Electron Microscopy. BEAS-2B cells were exposed to 50 μg/mL well-dispersed or poorly dispersed MWCNTs suspended in BEGM for 24 h. Harvested cells were fixed with 2% glutaraldehyde in 0.1 M phosphate-buffered saline (PBS) and washed.[53] After postfixation in 1% OsO_4 in PBS for 1 h, the cells were dehydrated in a graded ethanol series, treated with propylene oxide, and embedded in Epon. Approximately 50−70 nm thick sections were cut on a Reichert-Jung Ultracut E ultramicrotome and picked up on Formvar-coated copper grids. The sections were stained with uranyl acetate and Reynolds lead citrate and examined on a JEOL 100 CX transmission electron microscope at 80 kV in the UCLA BRI Electron Microscopy Core.

Mouse Exposure and Assessment of Exposure Outcomes in Mice. Eight week old male C57Bl/6 mice were purchased from Charles River Laboratories (Hollister, CA). All animals were housed under standard laboratory conditions that have been set up according to UCLA guidelines for care and treatment of laboratory animals as well as the NIH Guide for the Care and Use of Laboratory Animals in Research (DHEW78-23). These conditions are approved by the Chancellor's Animal Research Committee at UCLA and include standard operating procedures for animal housing (filter-topped cages; room temperature at 23 ± 2 °C; 60% relative humidity; 12 h light, 12 h dark cycle) and hygiene status (autoclaved food and acidified water). Animal exposures to well-dispersed or nondispersed tubes were carried out by an oropharyngeal aspiration method as described at NIOSH.[17] Briefly, the animals were anesthetized by intraperitoneal injection of ketamine (100 mg/kg)/xylazine (10 mg/kg) in a total volume of 100 μL. With the anesthetized animals held in a vertical position, a 50 μL PBS suspension containing 12.5−100 μg AP-MWCNTs was instilled at the back of the tongue to allow pulmonary aspiration. In a further experiment, all tube types, either in their dispersed or nondispersed states, were oropharyngeally administrated as a single bolus dose of 50 μg. Each experiment included control animals receiving the same volume of PBS with BSA (0.6 mg/mL) and DPPC (0.01 mg/mL). The positive control group in each experiment received 5 mg/kg crystalline silica in the form of quartz particles (Min-U-Sil). The mice were sacrificed 21 days later and bronchoalveolar lavage fluid (BALF) and lung tissue collected as previously described.[54] The BALF was used for performance of total and differential cell counts and to measure TGF-β1 and PDGF-AA levels. Lung tissue was stained with hematoxylin/eosin or with Masson's trichrome stain. Lung tissues were homogenized with a Tissuemiser homogenizer (Fisher Scientific) for the assessment of total collagen production (Sircol Collagen Assay, UK).[16,39]

Sircol Assay for Total Collagen Production. The right cranial lobe of each lung was suspended in PBS at around 50 mg tissue/mL and homogenized for 60 s with a tissue homogenizer (Fisher Scientific). Triton X-100 was added to 1% and the samples were incubated for 18 h at room temperature. Acetic acid was added to each sample to a final concentration of 0.5 M and incubated

at room temperature for 90 min. Cellular debris was pelleted by centrifugation and the supernatant analyzed for total protein, using a BCA assay kit (Pierce/ThermoFisher Scientific) according to manufacturer's instructions. The Sircol soluble collagen assay kit (Biocolor Ltd., Carrickfergus, UK) was used to extract collagen from duplicate samples using 200 μL of supernatant and 800 μL of Sircol dye reagent according to the manufacturer's instructions. Similarly prepared collagen standards (10−50 μg) were run in parallel. Collagen pellets were washed twice with denatured alcohol and dried before suspension in alkali reagent. Absorbance at 540 nm was read on a plate reader (SpectroMax M5e, Molecular Devices Corp., Sunnyvale, CA). Data were expressed as micrograms of soluble collagen per milligrams of total protein.

Airway Morphometry. Quantification of the thickness of collagen surrounding airways was performed according to a previously published airway intersect method.[26,36] Briefly, photomicrographs of trichrome-stained sections of lung tissue containing circular to oval-shaped small or medium-sized airways were captured using a 10× objective on an Olympus BX41 microscope (Olympus America Inc., Center Valley, PA) and digitized. The thickness of the collagen layer surrounding the airways was measured using the ruler tool in Adobe photoshop CS3 extended program (Adobe Systems, InC., San Jose, CA) at eight equidistant points and averaged. To validate the airway intersect measurements, a second independent method similar to a previously published method was used to measure the airway collagen area corrected for length of basement membrane (*i.e.*, area/perimeter ratio).[37] Briefly, the lasso tool in Adobe photoshop was used to surround the trichrome-positive collagen around an airway (outer area), then a second area measurement was made by surrounding the basement membrane of the same airway (inner area). Also, the length of the airway circumference (*i.e.*, perimeter) was also derived from this measurement. The difference between outer and inner area was defined as the "area" and divided by the "perimeter" to derive area/perimeter measurements. Both methods were performed in a blinded manner, where the treatment group was unknown to the observer scoring the sections. Five airways per animal were analyzed in a random, blinded manner, and the data were expressed as the mean 6 SEM of five animals per treatment group per time point.

ELISA for TGF-β1 and PDGF-AA Quantification. The TGF-β1 concentration in the BEAS-2B culture medium and the BALF was determined through the E_{max} ImmunoAssay system (Promega, Madison, WI, USA) according to the manufacturer's instruction. A 96-well plate was coated with monoclonal anti-TGF-β1 and the captured growth factor detected by polyclonal anti-TGF-β1 conjugated to horseradish peroxidase. Absorbance was measured at 450 nm using a plate reader (SpectroMax M5e, Molecular Devices Corp., Sunnyvale, CA, USA). PDGF-AA activity in the BALF was assessed by the Quantikine ELISA kit from R&D Systems (Minneapolis, MN) following the manufacturer's instructions. The supplied standard growth factor dilution series or 50 μL of BALF was pipetted into the anti-PDGF-AA precoated wells for antigen capture. After removal of the unbound growth factor by washing, an enzyme-linked anti-PDGF-AA monoclonal was added. Following washing to remove unbound secondary antibody, a substrate solution was added at 1:250 dilution for 30 min for color development. After termination of the color development, colometric intensity was measured at 450 nm in a plate reader (SpectroMax M5e, Molecular Devices Corp., Sunnyvale, CA, USA). The IL-1β activity in the THP-1 culture supernatant and the BALF was determined by an OptEIA (BD Biosciences, CA) ELISA kit according to the manufacturer's instructions. Briefly, a 96-well plate was coated with monoclonal anti-IL-1β and the immobilized growth factor detected by polyclonal anti-IL-1β conjugated to horseradish peroxidase. Absorbance was measured at 450 nm using a plate reader (SpectroMax M5e, Molecular Devices Corp., Sunnyvale, CA, USA). TGF-β1, PDGF-AA, and IL-1β concentrations were expressed as pg/mL.

Confocal Raman Microscopy in Cells and Lung Sections. Raman analysis was performed using backscattering geometry in a confocal configuration at room temperature in a Renishaw inVia Raman microscope system equipped with a 514.5 nm Ar laser. Laser power and beam size were approximately 2.5 mW and 1 μm, respectively, while the integration time was adjusted to 15 s. For cell sample preparation, BEAS-2B cells were cultured on sterile glass coverslips overnight and then exposed to well-dispersed AP-, PD-, and COOH-MWCNTs in BEGM (containing BSA and DPPC) for 24 h. Cells were washed three times in PBS and fixed with 4% paraformaldehyde in PBS for 30 min. The cells were scanned under the Raman microscope following three further washes in PBS. For lung tissue scanning, the lungs were fixed in paraffin, sectioned, and mounted onto glass slides without staining. The slides were dewaxed, hydrated, and then scanned under the confocal Raman microscope.

Statistical Analysis. Mean and standard deviation (SD) was calculated for each parameter. Results were expressed as mean ± SD of multiple determinations. Comparisons of each group were evaluated by two-side Student's *t* test. A statistically significant difference was assumed to exist when p was <0.05.

Acknowledgment. This work is supported by the U.S. Public Health Service Grants (RC2 ES018766, RO1 ES016746, and U19 ES019528). Infrastructure support was also provided by National Science Foundation and the Environmental Protection Agency under Cooperative Agreement Number, EF 0830117. Any opinions, findings, conclusions or recommendations expressed herein are those of the author(s) and do not necessarily reflect the views of the National Science Foundation or the Environmental Protection Agency. This work has not been subjected to an EPA peer and policy review. The findings and conclusions in this article are those of the authors and do not necessarily represent the views of the National Institute for Occupational Safety and Health.

Supporting Information Available: Additional experimental details. This material is available free of charge *via* the Internet at http://pubs.acs.org.

REFERENCES AND NOTES

1. Baughman, R. H.; Zakhidov, A. A.; de Heer, W. A. Carbon Nanotubes—The Route toward Applications. *Science* **2002**, *297*, 787–792.
2. Iijima, S. Helical Microtubules of Graphitic Carbon. *Nature* **1991**, *354*, 56–58.
3. Nel, A.; Xia, T.; Madler, L.; Li, N. Toxic Potential of Materials at the Nanolevel. *Science* **2006**, *311*, 622–627.
4. Kostarelos, K.; Bianco, A.; Prato, M. Promises, Facts and Challenges for Carbon Nanotubes in Imaging and Therapeutics. *Nat. Nanotechnol.* **2009**, *4*, 627–633.
5. Lin, Y.; Taylor, S.; Li, H. P.; Fernando, K. A. S.; Qu, L. W.; Wang, W.; Gu, L. R.; Zhou, B.; Sun, Y. P. Advances toward Bioapplications of Carbon Nanotubes. *J. Mater. Chem.* **2004**, *14*, 527–541.
6. Lam, C. W.; James, J. T.; McCluskey, R.; Hunter, R. L. Pulmonary Toxicity of Single-Wall Carbon Nanotubes in Mice 7 and 90 Days after Intratracheal Instillation. *Toxicol. Sci.* **2004**, *77*, 126–134.
7. Lee, J. H.; Lee, S. B.; Bae, G. N.; Jeon, K. S.; Yoon, J. U.; Ji, J. H.; Sung, J. H.; Lee, B. G.; Lee, J. H.; Yang, J. S.; *et al.* Exposure Assessment of Carbon Nanotube Manufacturing Workplaces. *Inhal. Toxicol.* **2010**, *22*, 369–381.
8. Muller, J.; Huaux, F.; Fonseca, A.; Nagy, J. B.; Moreau, N.; Delos, M.; Raymundo-Pinero, E.; Beguin, F.; Kirsch-Volders, M.; Fenoglio, I.; *et al.* Structural Defects Play a Major Role in the Acute Lung Toxicity of Multiwall Carbon Nanotubes: Toxicological Aspects. *Chem. Res. Toxicol.* **2008**, *21*, 1698–1705.
9. Oberdorster, G.; Maynard, A.; Donaldson, K.; Castranova, V.; Fitzpatrick, J.; Ausman, K.; Carter, J.; Karn, B.; Kreyling, W.; Lai, D.; *et al.* Principles for Characterizing the Potential Human Health Effects from Exposure to Nanomaterials: Elements of a Screening Strategy. *Part. Fibre Toxicol.* **2005**, *2*, 8.
10. Warheit, D. B.; Laurence, B. R.; Reed, K. L.; Roach, D. H.; Reynolds, G. A. M.; Webb, T. R. Comparative Pulmonary

Toxicity Assessment of Single-Wall Carbon Nanotubes in Rats. *Toxicol. Sci.* **2004**, *77*, 117–125.
11. Gao, N.; Zhang, Q.; Mu, Q.; Bai, Y.; Li, L.; Zhou, H.; Butch, E. R.; Powell, T. B.; Snyder, S. E.; Jiang, G.; *et al.* Steering Carbon Nanotubes to Scavenger Receptor Recognition by Nanotube Surface Chemistry Modification Partially Alleviates NFκB Activation and Reduces Its Immunotoxicity. *ACS Nano* **2011**, *5*, 4581–4591.
12. Liu, Z.; Tabakman, S.; Welsher, K.; Dai, H. J. Carbon Nanotubes in Biology and Medicine: *In Vitro* and *In Vivo* Detection, Imaging and Drug Delivery. *Nano Res.* **2009**, *2*, 85–120.
13. Maynard, A. D.; Baron, P. A.; Foley, M.; Shvedova, A. A.; Kisin, E. R.; Castranova, V. Exposure to Carbon Nanotube Material: Aerosol Release during the Handling of Unrefined Single-Walled Carbon Nanotube Material. *J. Toxicol. Environ. Health, Part A* **2004**, *67*, 87–107.
14. Mercer, R. R.; Hubbs, A. F.; Scabilloni, J. F.; Wang, L. Y.; Battelli, L. A.; Schwegler-Berry, D.; Castranova, V.; Porter, D. W. Distribution and Persistence of Pleural Penetrations by Multi-Walled Carbon Nanotubes. *Part. Fibre Toxicol.* **2010**, 7.
15. Muller, J.; Huaux, F.; Moreau, N.; Misson, P.; Heilier, J. F.; Delos, M.; Arras, M.; Fonseca, A.; Nagy, J. B.; Lison, D. Respiratory Toxicity of Multi-Wall Carbon Nanotubes. *Toxicol. Appl. Pharmacol.* **2005**, *207*, 221–231.
16. Ryman-Rasmussen, J. P.; Cesta, M. F.; Brody, A. R.; Shipley-Phillips, J. K.; Everitt, J. I.; Tewksbury, E. W.; Moss, O. R.; Wong, B. A.; Dodd, D. E.; Andersen, M. E.; *et al.* Inhaled Carbon Nanotubes Reach the Subpleural Tissue in Mice. *Nat. Nanotechnol.* **2009**, *4*, 747–751.
17. Shvedova, A. A.; Kisin, E.; Murray, A. R.; Johnson, V. J.; Gorelik, O.; Arepalli, S.; Hubbs, A. F.; Mercer, R. R.; Keohavong, P.; Sussman, N.; *et al.* Inhalation *vs.* Aspiration of Single-Walled Carbon Nanotubes in C57BL/6 Mice: Inflammation, Fibrosis, Oxidative Stress, and Mutagenesis. *Am. J. Physiol. Lung. Cell. Mol. Physiol.* **2008**, *295*, L552–L565.
18. Shvedova, A. A.; Kisin, E. R.; Mercer, R.; Murray, A. R.; Johnson, V. J.; Potapovich, A. I.; Tyurina, Y. Y.; Gorelik, O.; Arepalli, S.; Schwegler-Berry, D.; *et al.* Unusual Inflammatory and Fibrogenic Pulmonary Responses to Single-Walled Carbon Nanotubes in Mice. *Am. J. Physiol. Lung Cell. Mol. Physiol.* **2005**, *289*, L698–L708.
19. Pauluhn, J. Multi-Walled Carbon Nanotubes (Baytubes (R)): Approach for Derivation of Occupational Exposure Limit. *Regul. Toxicol. Pharmacol.* **2010**, *57*, 78–89.
20. Porter, D. W.; Hubbs, A. F.; Mercer, R. R.; Wu, N. Q.; Wolfarth, M. G.; Sriram, K.; Leonard, S.; Battelli, L.; Schwegler-Berry, D.; Friend, S.; *et al.* Mouse Pulmonary Dose- and Time Course-Responses Induced by Exposure to Multi-Walled Carbon Nanotubes. *Toxicology* **2010**, *269*, 136–147.
21. Deng, X.; Jia, G.; Wang, H.; Sun, H.; Wang, X.; Yang, S.; Wang, T.; Liu, Y. Translocation and Fate of Multi-Walled Carbon Nanotubes *in Vivo*. *Carbon* **2007**, *45*, 1419–1424.
22. Mercer, R. R.; Scabilloni, J.; Wang, L.; Kisin, E.; Murray, A. R.; Schwegler-Berry, D.; Shvedova, A. A.; Castranova, V. Alteration of Deposition Pattern and Pulmonary Response as a Result of Improved Dispersion of Aspirated Single-Walled Carbon Nanotubes in a Mouse Model. *Am. J. Physiol. Lung. Cell. Mol. Physiol.* **2008**, *294*, L87–L97.
23. Jia, G.; Wang, H. F.; Yan, L.; Wang, X.; Pei, R. J.; Yan, T.; Zhao, Y. L.; Guo, X. B. Cytotoxicity of Carbon Nanomaterials: Single-Wall Nanotube, Multi-Wall Nanotube, and Fullerene. *Environ. Sci. Technol.* **2005**, *39*, 1378–1383.
24. Nel, A. E.; Madler, L.; Velegol, D.; Xia, T.; Hoek, E. M. V.; Somasundaran, P.; Klaessig, F.; Castranova, V.; Thompson, M. Understanding Biophysicochemical Interactions at the Nano-Bio Interface. *Nat. Mater.* **2009**, *8*, 543–557.
25. Poland, C. A.; Duffin, R.; Kinloch, I.; Maynard, A.; Wallace, W. A. H.; Seaton, A.; Stone, V.; Brown, S.; MacNee, W.; Donaldson, K. Carbon Nanotubes Introduced into the Abdominal Cavity of Mice Show Asbestos-like Pathogenicity in a Pilot Study. *Nat. Nanotechnol.* **2008**, *3*, 423–428.
26. Ryman-Rasmussen, J. P.; Tewksbury, E. W.; Moss, O. R.; Cesta, M. F.; Wong, B. A.; Bonner, J. C. Inhaled Multiwalled Carbon Nanotubes Potentiate Airway Fibrosis in Murine Allergic Asthma. *Am. J. Respir. Cell Mol. Biol.* **2009**, *40*, 349–358.
27. Donaldson, K.; Murphy, F. A.; Duffin, R.; Poland, C. A. Asbestos, Carbon Nanotubes and the Pleural Mesothelium: A Review of the Hypothesis Regarding the Role of Long Fibre Retention in the Parietal Pleura, Inflammation and Mesothelioma. *Part. Fibre Toxicol.* **2010**, 7.
28. Tschopp, J.; Dostert, C.; Petrilli, V.; Van Bruggen, R.; Steele, C.; Mossman, B. T. Innate Immune Activation through Nalp3 Inflammasome Sensing of Asbestos and Silica. *Science* **2008**, *320*, 674–677.
29. Tschopp, J.; Schroder, K. NLRP3 Inflammasome Activation: the Convergence of Multiple Signalling Pathways on ROS Production? *Nat. Rev. Immunol.* **2010**, *10*, 210–215.
30. Tschopp, J.; Schroder, K.; Zhou, R. B. The NLRP3 Inflammasome: A Sensor for Metabolic Danger? *Science* **2010**, *327*, 296–300.
31. Wang, L. Y.; Castranova, V.; Mishra, A.; Chen, B.; Mercer, R. R.; Schwegler-Berry, D.; Rojanasakul, Y. Dispersion of Single-Walled Carbon Nanotubes by a Natural Lung Surfactant For Pulmonary *In Vitro* and *In Vivo* Toxicity Studies. *Part. Fibre Toxicol.* **2010**, 7.
32. Bonner, J. C. Mesenchymal Cell Survival in Airway and Interstitial Pulmonary Fibrosis. *Fibrogenesis Tissue Repair* **2010**, *3*, 15.
33. Bonner, J. C. Regulation of PDGF and Its Receptors in Fibrotic Diseases. *Cytokine Growth Factor Rev.* **2004**, *15*, 255–273.
34. Chapman, H. A. Epithelial−Mesenchymal Interactions in Pulmonary Fibrosis. *Annu. Rev. Physiol.* **2010**, *73*, 413–435.
35. Wang, X.; Xia, T.; Ntim, S. A.; Ji, Z. X.; George, S.; Meng, H.; Zhang, H. Y.; Castranova, V.; Mitra, S.; Nel, A. E. Quantitative Techniques for Assessing and Controlling the Dispersion and Biological Effects of Multiwalled Carbon Nanotubes in Mammalian Tissue Culture Cells. *ACS Nano* **2010**, *4*, 7241–7252.
36. Card, J. W.; Voltz, J. W.; Carey, M. A.; Bradbury, J. A.; Degraff, L. M.; Lih, F. B.; Bonner, J. C.; Morgan, D. L.; Flake, G. P.; Zeldin, D. C. Cyclooxygenase-2 Deficiency Exacerbates Bleomycin-Induced Lung Dysfunction but Not Fibrosis. *Am. J. Respir. Cell Mol. Biol.* **2007**, *37*, 300–308.
37. Brass, D. M.; Savov, J. D.; Gavett, S. H.; Haykal-Coates, N.; Schwartz, D. A. Subchronic Endotoxin Inhalation Causes Persistent Airway Disease. *Am. J. Physiol. Lung. Cell. Mol. Physiol.* **2003**, *285*, L755–L761.
38. Wang, L.; Mercer, R. R.; Rojanasakul, Y.; Qiu, A.; Lu, Y.; Scabilloni, J. F.; Wu, N.; Castranova, V. Direct Fibrogenic Effects of Dispersed Single-Walled Carbon Nanotubes on Human Lung Fibroblasts. *J. Toxicol. Environ. Health A* **2010**, *73*, 410–422.
39. Mutlu, G. M.; Budinger, G. R. S.; Green, A. A.; Urich, D.; Soberanes, S.; Chiarella, S. E.; Alheid, G. F.; McCrimmon, D. R.; Szleifer, I.; Hersam, M. C. Biocompatible Nanoscale Dispersion of Single-Walled Carbon Nanotubes Minimizes *In Vivo* Pulmonary Toxicity. *Nano Lett.* **2010**, *10*, 1664–1670.
40. Wang, X.; Jia, G.; Wang, H.; Nie, H.; Yan, L.; Deng, X. Y.; Wang, S. Diameter Effects on Cytotoxicity of Multi-Walled Carbon Nanotubes. *J. Nanosci. Nanotechnol.* **2009**, *9*, 3025–3033.
41. Wang, X.; Zang, J. J.; Wang, H.; Nie, H.; Wang, T. C.; Deng, X. Y.; Gu, Y. Q.; Liu, Z. H.; Jia, G. Pulmonary Toxicity in Mice Exposed to Low and Medium Doses of Water-Soluble Multi-Walled Carbon Nanotubes. *J. Nanosci. Nanotechnol.* **2010**, *10*, 8516–8526.
42. Xia, T.; Zhao, Y.; Sager, T.; George, S.; Pokhrel, S.; Li, N.; Schoenfeld, D.; Meng, H.; Lin, S. J.; Wang, X.; *et al.* Decreased Dissolution of ZnO by Iron Doping Yields Nanoparticles with Reduced Toxicity in the Rodent Lung and Zebrafish Embryos. *ACS Nano* **2011**, *5*, 1223–1235.
43. Meng, H.; Xia, T.; George, S.; Nel, A. E. A Predictive Toxicological Paradigm for the Safety Assessment of Nanomaterials. *ACS Nano* **2009**, *3*, 1620–1627.

44. George, S.; Pokhrel, S.; Xia, T.; Gilbert, B.; Ji, Z. X.; Schowalter, M.; Rosenauer, A.; Damoiseaux, R.; Bradley, K. A.; Madler, L.; *et al.* Use of a Rapid Cytotoxicity Screening Approach To Engineer a Safer Zinc Oxide Nanoparticle through Iron Doping. *ACS Nano* **2010**, *4*, 15–29.
45. Han, J. H.; Lee, E. J.; Lee, J. H.; So, K. P.; Lee, Y. H.; Bae, G. N.; Lee, S. B.; Ji, J. H.; Cho, M. H.; Yu, I. J. Monitoring Multiwalled Carbon Nanotube Exposure in Carbon Nanotube Research Facility. *Inhal. Toxicol.* **2008**, *20*, 741–749.
46. Stone, K. C.; Mercer, R. R.; Gehr, P.; Stockstill, B.; Crapo, J. D. Allometric Relationships of Cell Numbers and Size in the Mammalian Lung. *Am. J. Respir. Cell Mol. Biol.* **1992**, *6*, 235–243.
47. NIOSH Current Intelligence Bulletin: Occupational Exposure to Carbon Nanotubes, 2011; www.cdc.gov/niosh/docket/review/docket161A/.
48. Wang, Y.; Iqbal, Z.; Mitra, S. Rapid, Low Temperature Microwave Synthesis of Novel Carbon Nano Tube-Silicon Carbide Composite. *Carbon* **2006**, *44*, 2804–2808.
49. Wang, Y. B.; Iqbal, Z.; Mitra, S. Microwave-Induced Rapid Chemical Functionalization of Single-Walled Carbon Nanotubes. *Carbon* **2005**, *43*, 1015–1020.
50. Wang, Y. B.; Iqbal, Z.; Mitra, S. Rapidly Functionalized, Water-Dispersed Carbon Nanotubes at High Concentration. *J. Am. Chem. Soc.* **2006**, *128*, 95–99.
51. Deguchi, S.; Yamazaki, T.; Mukai, S.; Usami, R.; Horikoshi, K. Stabilization of C-60 Nanoparticles by Protein Adsorption and Its Implications for Toxicity Studies. *Chem. Res. Toxicol.* **2007**, *20*, 854–858.
52. Thess, A.; Lee, R.; Nikolaev, P.; Dai, H. J.; Petit, P.; Robert, J.; Xu, C. H.; Lee, Y. H.; Kim, S. G.; Rinzler, A. G.; *et al.* Crystalline Ropes of Metallic Carbon Nanotubes. *Science* **1996**, *273*, 483–487.
53. Xia, T.; Kovochich, M.; Liong, M.; Zink, J. I.; Nel, A. E. Cationic Polystyrene Nanosphere Toxicity Depends on Cell-Specific Endocytic and Mitochondrial Injury Pathways. *ACS Nano* **2008**, *2*, 85–96.
54. Li, N.; Wang, M. Y.; Bramble, L. A.; Schmitz, D. A.; Schauer, J. J.; Sioutas, C.; Harkema, J. R.; Nel, A. E. The Adjuvant Effect of Ambient Particulate Matter Is Closely Reflected by the Particulate Oxidant Potential. *Environ. Health Perspect.* **2009**, *117*, 1116–1123.